

**THE HETEROGENATION OF IRON-CARBONYL
THIOUREA COMPLEX ONTO RICE HUSK
SILICA AND ITS CATALYTIC OXIDATION OF
LIMONENE WITH HYDROGEN PEROXIDE**

NADIAH BTE AMERAM

UNIVERSITI SAINS MALAYSIA

2017

**THE HETEROGENATION OF IRON-CARBONYL
THIOUREA COMPLEX ONTO RICE HUSK
SILICA AND ITS CATALYTIC OXIDATION OF
LIMONENE WITH HYDROGEN PEROXIDE.**

by

NADIAH BTE AMERAM

**Thesis submitted in fulfillment of the requirements
for the degree of
Doctor of Philosophy**

August 2017

ACKNOWLEDGEMENT

In The Name of Allah, Most Gracious, Most Merciful

This work could not have been completed without the help of many individuals. I would like to start by expressing my utmost gratitude to the government of Malaysia, University of Science Malaysia for financially supporting me throughout my studies of the RU grants (1001/PKIMIA/846017), (1001/PKIMIA/811269) and University of Malaysia Kelantan.

I would like to convey my sincerest appreciation to my supportive supervisor, Prof Farook Adam. I would like to thank my supervisor for his continuous support and academic advices in enhancing my skills and in the completion of my PhD which has been an excellent learning experience. He has always taught me to think from different perspectives when solving an issue. He has also taught me to be optimistic and tenacious in order to achieve my goals.

Many thanks to the staff of Institute of Postgraduate studies (IPS), School of Chemical Science, School of Physics and School of Biological Sciences, USM for assisting me the use of the necessary equipment and analysis.

I also thank the previous and current members of the heterogenous catalysis labmates for their helps, the knowledge sharing and instilling confidence.

Finally, I would like to share my deepest appreciation to my family for their constant support for me and for always believing in me. They are the most important individuals in my world and I am dedicating this thesis to them. Especially my mother (Pn. Zaleha) who had looked after my daughter (Cik Najlaa') while I was pursuing my studies. Utmost gratitude for my husband (En. Ahmad Najme) and all of my siblings who have always pray for my success. Thank you all so much. Praise is due to Allah whose worth cannot be described by speakers.

TABLE OF CONTENTS

Acknowledgement.....	ii
Table of Content.....	iii
List of Figures.....	x
List of Tables.....	xxi
List of Scheme.....	xxv
List of Symbol	xxvii
List of Abbreviations.....	xxviii
Abstrak.....	xxx
Abstract.....	xxxi

CHAPTER 1-INTRODUCTION

1.1	General Introduction.....	1
1.2	Silica.....	1
1.2.1	Silica in rice husk (RH) and rice husk ash (RHA).....	3
1.2.2	The silanol and siloxane bonds in RHA.....	4
1.3	Organically functionalized mesoporous materials.....	6
1.4	Hydrogen bonded urea and hydrogen peroxide	8
1.5	Thiourea.....	10
1.5.1	Introduction to thiourea.....	10
1.5.2	Thione–thiol tautomerism.....	11
1.5.3	The metal transition complexes of thiourea.....	12
1.5.4	Iron.....	13
1.5.5	Thiourea immobilised silica as a support.....	14
1.5.6	Literature Review of Thiourea Derivatives.....	16
1.6	Primary, secondary and tertiary amine in reactions.....	19
1.7	Limonene.....	19
1.8	Oxidation of Limonene.....	21
1.9	Problem Statement.....	27
1.10	Objectives of the study.....	29

CHAPTER 2- EXPERIMENTAL

2.1	Chemicals.....	30
2.2	Extraction of silica from RH.....	31
2.2.1	Washing of RH.....	31
2.2.2	Acid treatment of rice husk.....	31
2.2.3	Preparation of sodium silicate solution.....	32
2.3	Synthesis of the organic ligand.....	32
2.3.1	Synthesis of 2-methyl- <i>N</i> -[(2-pyridine-2-yl-ethyl) carbamothio- yl]benzamide, O2.....	33
2.3.2	Synthesis of 4-methyl- <i>N</i> -[(4-methylpyridin-2-yl)carbamothioy -l]benzamide, P1.....	34
2.3.3	Synthesis of 4-methyl- <i>N</i> -[(2-pyridine-2-yl-ethyl) carbamothioyl]benzamide, P2.....	34
2.3.4	Synthesis of metal complex, [Fe(P1)]Cl.....	34
2.4	Preparation of the catalyst.....	36
2.4.1	Preparation of RHACCl.....	36
2.4.2	Functionalization of O2 onto silica.....	37
2.4.3	Preparation of RHACP2, RHACP1 and RHACP1Fe.....	38
2.5	Characterization and analysis.....	39
2.5.1	Physico–chemical characterization.....	39
2.5.2	Fourier transform infrared spectroscopy (FT-IR).....	40
2.5.3	Carbon, Hydrogen, Nitrogen (CHN) analysis.....	40
2.5.4	Nitrogen adsorption-desorption analysis.....	41
2.5.5	Thermogravimetric analysis (TGA)/Differential thermal analysis (DTA).....	41
2.5.6	Powder X–Ray diffraction (XRD).....	42
2.5.7	²⁹ Si CP/MAS NMR spectroscopy.....	42
2.5.8	¹³ C CP/MAS NMR spectroscopy.....	43
2.5.9	¹ H liquid state NMR spectroscopy.....	43
2.5.1	¹³ C liquid state NMR spectroscopy.....	43
2.5.1	Scanning Electron Microscopy–Energy Dispersive X–ray (SEM/EDX).....	44
2.5.1	Transmission Electron Microscopy (TEM).....	44
2.5.1	X-ray crystallography.....	45

2.5.1	Atomic absorption spectroscopy (AAS) analysis.....	45
2.6	Catalytic reactions.....	46
2.6.1	General reaction procedures.....	46
2.6.2	Gas chromatography (GC) and Gas chromatography-mass spectroscopy (GC-MS).....	47

CHAPTER 3- CHARACTERIZATION OF ORGANIC LIGANDS

3.1	Introduction.....	48
3.2	2-methyl- <i>N</i> -[(2-pyridine-2-yl-ethyl)carbamothioyl]benzamide.....	48
3.2.1	X-Ray Chrystallography.....	48
3.2.2	Fourier transformed infrared spectroscopy (FT-IR).....	53
3.2.3	Liquid state ^1H NMR spectroscopy.....	55
3.2.4	Liquid state ^{13}C NMR spectroscopy.....	58
3.2.5	Elemental analysis (CHN).....	59
3.3	4-methyl- <i>N</i> -[(4-methylpyridin-2-yl)carbamothioyl]benzamide.....	60
3.3.1	X-Ray Chrystallography.....	60
3.3.2	Fourier transformed infrared spectroscopy (FT-IR).....	60
3.3.3	Liquid state ^1H NMR spectroscopy.....	64
3.3.4	Liquid state ^{13}C NMR spectroscopy.....	65
3.3.5	Elemental analysis (CHN).....	67
3.4	4-methyl- <i>N</i> -[(2-pyridine-2-yl-ethyl)carbamothioyl]benzamide.....	70
3.4.1	X-Ray Chrystallography.....	70
3.4.2	Fourier transformed infrared spectroscopy (FT-IR).....	70
3.4.3	Liquid state ^1H NMR spectroscopy.....	75
3.4.4	Liquid state ^{13}C NMR spectroscopy.....	77
3.4.5	Elemental analysis (CHN).....	81
3.5	[Fe(P1)]Cl.....	83
3.5.1	Fourier transformed infrared spectroscopy (FT-IR) of [Fe(P1)]Cl.....	84
3.5.2	Liquid state ^1H NMR spectroscopy.....	85
3.5.3	Liquid state ^{13}C NMR spectrum of [Fe(P1)]Cl.....	86
3.5.4	Elemental analysis (CHN).....	89

CHAPTER 4-THE HETEROGENATION OF O₂, P1 AND P2 ON SILICA

4.1	Introduction.....	90
4.2	The synthesis and characterization of RHACO ₂	91
4.2.1	Elemental analysis.....	90
4.2.2	The Nitrogen adsorption analysis.....	92
4.2.3	FT-IR Spectrum of RHACO ₂	93
4.2.4	Powder X-ray Diffraction (XRD).....	96
4.2.5	Solid-state MAS NMR.....	96
	4.2.5(a) The ²⁹ Si MAS NMR.....	96
	4.2.5(b) The ¹³ C MAS NMR.....	98
4.2.6	Electron Microscope (TEM/SEM).....	101
4.2.7	Thermogravimetric Analysis (TGA/DTA).....	102
4.3	Introduction	103
4.4	Characterization of RHACP1.....	103
4.4.1	Elemental Analysis	103
4.4.2	The Nitrogen adsorption-desorption analysis.....	103
4.4.3	Thermogravimetric (TGA) and differential thermal analyses (DTA).....	105
4.4.4	The FT-IR spectrum of RHACP1.....	107
4.4.5	Powder X-ray Diffraction (XRD).....	108
4.4.6	Solid-state MAS NMR	
	4.46 (a) Solid-state ²⁹ Si MAS NMR	111
	4.46 (b) Solid-state ¹³ C MAS NMR.....	111
4.4.7	Determination of percentages of organic loading.....	114
4.4.8	Electron microscopic analysis (SEM and TEM).....	115
4.5	The synthesis and characterization of solid P2 catalyst, RHACP2..	114
4.5.1	Elemental/ EDX analysis.....	116
4.5.2	The Nitrogen adsorption analysis	117
4.5.3	Thermogravimetric analysis (TGA) and Differential thermal analysis (DTA).....	118
4.5.4	Powder X-ray Diffraction (XRD).....	120
4.5.5	Fourier Transformed Infrared spectroscopy analysis (FT-IR)....	120
4.5.6	Solid-state MAS NMR.....	122

4.5.6 (a)	The ^{29}Si MAS NMR.....	122
4.5.6 (b)	The ^{13}C CP/MAS NMR.....	126
4.5.7	Electron micrographs (SEM and TEM).....	127

CHAPTER 5- CATALYTIC ACTIVITY OF HETEROGENEOUS ORGANIC LIGAND (O2), (P1) and (P2)

5.1	Introduction.....	129
5.1.1	The effect of reaction time on the percentage conversion of limonene	130
5.1.1	Effect of catalyst amount.....	131
5.1.2	Effect of H_2O_2 concentration on the oxidation of limonene.....	132
5.1.3	Effect of H_2O_2 concentration on the oxidation of limonene.....	134
5.1.4	The effect of reaction temperature on the percentage conversion of limonene and product selectivity	135
5.1.5	Effect of O_2 ligand as a homogeneous catalyst versus the heterogeneous RHACO_2	137
5.1.6	Reusability	138
5.1.7	Re-characterization of used RHACO_2	138
	5.17 (a) Powder X-ray diffraction (XRD).....	
	5.17 (b) Transmission Electron Microscope.....	
5.1.8	The proposed mechanism of limonene oxidation.....	138
5.1.9	Summary	139
5.2	Oxidation of Limonene by using RHACP1	141
5.2.1	The effect of reaction time on the percentage conversion of limonene.....	142
5.2.2	Effect of catalyst amount.....	143
5.2.3	Effect of H_2O_2 concentration on the oxidation of limonene.....	144
5.2.4	The effect of reaction temperature on the percentage conversion of limonene and product selectivity.....	146
5.2.5	Effect of P1 ligand as a homogeneous catalyst versus the heterogeneous RHACP1	147
5.2.6	Reusability.....	148
5.2.7	Re-characterization of used RHACP1	149

5.2.7 (a)	Powder X-ray diffraction (XRD).....	149
5.2.7 (b)	Transmission Electron Microscope.....	149
5.2.8	The proposed mechanism of limonene oxidation.....	150
5.2.9	Summary.....	151
5.3	Oxidation of Limonene by using RHACP2.....	152
5.3.1	The effect of reaction time on the percentage conversion of limonene.....	153
5.3.2	Effect of catalyst amount.....	154
5.3.3	Effect of H ₂ O ₂ concentration on the oxidation of limonene.....	155
5.3.4	The effect of reaction temperature on the percentage..... Conversion of limonene and product selectivity.....	156
5.3.5	Effect of P2 ligand as a homogeneous catalyst versus the heterogeneous RHACP2 catalyst.....	157
5.3.6	Reusability.....	159
5.3.7	Re-characterization of used RHACP2.....	160
5.3.8 (a)	Powder X-ray diffraction (XRD).....	160
5.3.8 (b)	Transmission Electron Microscope.....	160
5.3.8	The proposed mechanism of limonene oxidation.....	161
5.3.9	Summary.....	162

CHAPTER 6- THE SYNTHESIS, CHARACTERIZATION AND CATALYTIC ACTIVITY OF HETEROGENEOUS METAL COMPLEX ([Fe(P1)]Cl)

6.1	The synthesis and characterization of solid P1Fe catalyst, RHACP1Fe.	165
6.2	The EDX analysis.....	166
6.3	The Nitrogen adsorption analysis.....	167
6.4	Powder X-ray Diffraction (XRD).....	167
6.4	FT-IR Spectrum.....	168
6.5	Solid-state MAS NMR.....	169
6.5.1	The ²⁹ Si MAS NMR.....	169
6.5.2	The ¹³ C MAS NMR.....	169
6.6	Electron micrographs (SEM and TEM).....	170
6.6.1	The ²⁹ Si MAS NMR.....	170

6.7	Thermogravimetric analysis (TGA).....	175
6.9	Oxidation of Limonene by using RHACP1Fe.....	176
6.10	The effect of reaction time on percentage conversion of limonene.....	176
6.11	Effect of catalyst amount.....	177
6.12	Effect of H ₂ O ₂ concentration on the oxidation of limonene.....	179
6.13	The effect of reaction temperature on the percentage conversion of limonene and product selectivity.....	180
6.14	Reusability.....	181
6.15	Effect of metal support in reaction.....	182
6.16	Re-characterization of used RHACP1Fe.....	183
6.16.1	Powder X-ray diffraction (XRD).....	183
6.16.2	Transmission Electron Microscope.....	184
6.17	The proposed mechanism of limonene oxidation.....	184
6.18	Summary.....	185
 CHAPTER 7- CONCLUSION AND FUTURE STUDIES		
7.1	Conclusion and Recommendation.....	196
7.2	Probable Future Works.....	199
 REFERENCES.....		200
APPENDICES		

LIST OF FIGURES

		Page
Fig. 1.1	The conversion of rice husk to rice husk ash (RHA).....	4
Fig. 1.2	Different forms of silanol groups at the silica surface (Sharma et al. 2015).....	5
Fig. 1.3	The silica surface with various bridging formation to the silicon of propylsilane. The nature of the T ¹ , T ² and T ³ silicon atoms in the immobilized silica.....	6
Fig. 1.4	Three synthesis approaches for the synthesis of mesoporous hybrid materials (Hoffnam et al. 2006).....	7
Fig. 1.5	Synthesis of metal complex at the beginning of the reaction.	9
Fig. 1.6	Hydrogen bonded complex of urea and hydrogen peroxide (UHP).....	9
Fig. 1.7	Structure of urea and thiourea	10
Fig. 1.8	General structure of benzoylthiourea.....	10
Fig. 1.9	Thione–thiol tautomerism in acylthioureas.....	11
Fig.1.10	Typical Hydrogen-Bonding Modes of Urea/Thiourea Molecules: (a) Head to-Tail; (b) Shoulder-to-Shoulder; (c) Designation of syn- and anti-Hydrogen Atoms.....	11
Fig. 1.11	Neutral monodentate through the S atom (left) and monobasic O, S bidentate (right) coordination modes found in Pd(II) complexes of 1-(benzoyl)-3, 3-(di-alkyl) thioureas. Adapted from reference (Karipcin et al., 2011).....	12

Fig. 1.12	Cooperative catalysis by acid and base bifunctionalized MSN.....	14
Fig. 1.13	Scheme of secondary and tertiary amine in reactions.....	19
Fig. 1.14	Orange essential oil from orange peel obtained at room temperature after centrifugation of the water oil emulsion. (Image courtesy of (Pourbafrani et al., 2010)).....	20
Fig.1.15	Stereoisomer of limonene with chiral center denoted as (*) at carbon 4.....	20
Fig. 3.1	The molecular structure of the title compound, with atom labelling. Displacement ellipsoids are drawn at the 50 % probability level. The intra-molecular N-H ···O hydrogen bond is shown as a dashed line.....	50
Fig. 3.2	A view along the a axis of the crystal packing of the title compound. The hydrogen bonds and C-H ···p interactions (H atoms grey ball) are shown as dashed lines...	52
Fig. 3.3	The FT-IR spectrum of 2-methyl-N-[(2-pyridine-2-yl-ethyl) carbamothioyl]benzamide.....	54
Fig.3.4	The ¹ H NMR spectrum of 2-methyl-N-[(2-pyridine-2-yl-ethyl)carbamothioyl]benzamide.....	57
Fig. 3.5	¹³ C NMR for 2-methyl-N- [(2-pyridine-2-yl-ethyl) carbamothioyl]benzamide.....	59
Fig. 3.6	The molecular structure of 2-methyl-N-[(2-pyridine-2-yl-ethyl)carbamothiol]benzamide, with 50 % probability displacement ellipsoids. Hydrogen bonds are shown as	

	dashed lines.....	61
Fig. 3.7	The crystal packing of ethyl- <i>N</i> -[(2-pyridine-2-yl-ethyl) carbamothioyl]benzamide compound is viewed down the c-axis. Hydrogen bonds are shown as dashed lines.....	62
Fig. 3.8	FTIR spectrum of 4-methyl- <i>N</i> -[(4-methylpyridin-2-yl) carbamothioyl]benzamide.....	65
Fig.3.9	The ¹ H NMR of 4-methyl- <i>N</i> -[(4-methylpyridin-2-yl) carbamothioyl]benzamide.....	67
Fig. 3.10	¹³ C NMR for 4-methyl- <i>N</i> -[(4-methylpyridin-2-yl) carbamothioyl]benzamide	69
Fig. 3.11	The X-ray crystal structure of 4-methyl- <i>N</i> - [(2-pyridine-2-yl-etthyl)carbamothioyl] benzamide. The dashed line indicates hydrogen bonds.....	72
Fig. 3.12	The crystal packing of 4-methyl- <i>N</i> -[(2-pyridine-2-yl-ethyl) carbamothioyl]benzamide viewed along b-axis.....	75
Fig. 3.13	The FT-IR spectrum of 4-methyl- <i>N</i> -[(2-pyridine-2-yl-ethyl) carbamothioyl]benzamide.....	76
Fig. 3.14	The ¹ H NMR spectrum of 4-methyl- <i>N</i> -[(2-pyridine-2-yl-ethyl)carbamothioyl]benzamide.....	79
Fig. 3.15	Enhanced of ¹ H NMR spectrum of 4-methyl- <i>N</i> -[(2 -pyridine-2-yl-ethyl)carbamothioyl] benzamide.....	80
Fig. 3.16	¹³ C NMR for 4- methyl- <i>N</i> - [(2-pyridine-2-yl-ethyl)carbamothioyl]benzamide (II) [P2].....	82

Fig. 3.17	Proposed structure of P1 metal complex, [Fe(P1)]Cl.....	83
Fig.3.18	The FT-IR spectrum of [Fe(P1)]Cl.....	84
Fig. 3.19	The ^1H NMR spectrum of [Fe(P1)]Cl.....	87
Fig. 3.20	The ^{13}C NMR spectrum of [Fe(P1)]Cl.....	88
Fig. 4.1	(a) The EDX analysis showed the presence of nitrogen in RHACO2 (b) The EDX analysis of RHACCl.....	91
Fig. 4.2	(a) The nitrogen adsorption /desorption isotherms of RHACO2. (b) The corresponding pore size distribution.....	93
Fig. 4.3	The FTIR spectra of RHACCl, RHACO2 and their differential spectrum.....	94
Fig. 4.4	The X-ray diffraction pattern show amorphous nature of RHACO2.....	99
Fig. 4.5	The ^{29}Si MAS NMR solid-state spectrum of RHACO2. The Chemical shifts of T^2 , T^3 , Q^3 and Q^4 are observed. The inset show ^{29}Si MAS NMR solid-state spectrum of RHACCl.....	97
Fig. 4.6	The possible structures for RHACO2 as suggested by MAS NMR and FT-IR. (a) T^3 - three siloxane bonds to silicon, (b) T^2 -two siloxane bonds to silicon.....	96
Fig. 4.7	The solid state ^{13}C MAS NMR spectra for RHACO2 at the Spinning rate of 5 KHz.....	100
Fig. 4.8	The SEM micrograph of RHACO2 at different magnification ca (a) at 500 and (b) 15 k.....	101

Fig. 4.9	The TEM micrograph of RHACO2 at different magnification ca. (a) at 100 k and (b) 120 k.....	101
Fig. 4.10	Thermogravimetric analysis of RHACO2.....	102
Fig. 4.11	The EDX analysis showed the presence of sulphur, nitrogen and oxygen in RHACP1.....	104
Fig. 4.12	The nitrogen adsorption/desorption isotherms of RHACP1. (b) Pore size distribution for RHACP1.....	106
Fig. 4.13	Thermogravimetric and differential thermal analyses plots of RHACP1.....	108
Fig. 4.14	The FT-IR spectra of RHACCl, RHACP1 and differential spectrum.....	110
Fig. 4.15	The X-ray diffraction pattern shows amorphous nature of RHACP1.....	111
Fig. 4.16	The ^{29}Si MAS NMR solid-state spectrum of RHACP1. The chemical shifts T^1 , T^2 , Q^2 and Q^3 are observed (Inset shows the ^{29}Si for RHACCl).....	112
Fig. 4.17	The possible structures for RHACP1 as suggested by MAS NMR and FTIR (a) T^1 -one siloxane bonds to silicon, (b) T^2 - two siloxane bonds to silicon.....	112
Fig. 4.18	The solid state ^{13}C MAS NMR spectra for RHACP1 at 5 KHz.....	113
Fig. 4.19	The SEM micrograph of RHACP1 at different magnification ca. (a) at 5 k and (b) 30 k.....	114

Fig. 4.20	The TEM micrograph of RHACP1 at different magnification ca. (a) at 100 k and (b) 120 k.....	115
Fig. 4.21	The EDX analysis showed the presence of nitrogen in RHACP2.....	116
Fig. 4.22	The nitrogen adsorption/desorption isotherms of RHACP2. The inset shows the corresponding pore size distribution....	117
Fig. 4.23	Thermogravimetric analysis (TGA/DTA) for RHACP2. Five characteristic decomposition stages are shown	119
Fig. 4.24	The X-ray diffraction pattern shows amorphous nature of RHACP2.....	120
Fig. 4.25	The FT-IR spectra of RHACC1, RHACP2 and differential..	121
Fig. 4.26	The solid state ^{29}Si C/P MAS NMR spectrum for RHACP2.	124
Fig. 4.27	The possible structures for RHACP2 as suggested by MAS NMR and FTIR. (a) T^2 - two siloxane bonded to silicon, (b) T^1 - one siloxane bonded to silicon.....	125
Fig. 4.28	The solid state ^{13}C MAS NMR spectrum for RHACP2.....	126
Fig. 4.29	The SEM images of RHACP2 at ca. (a) 5 k magnification, (b) 30 k magnification.....	128
Fig. 4.30	The TEM images of RHACP2 at (a) 200 k (b) 600 k magnification.....	128
Fig. 5.1	Conversion of limonene versus reaction time with 0.30 g	

	Catalyst, and 1:1 molar ratio at a reaction temperature of 80 °C.....	130
Fig. 5.2	The effect of catalyst mass on the oxidation of limonene. Reaction condition: molar ratio of limonene: H ₂ O ₂ = 1:1, 4h of reaction, 80 °C. LG: limonene glycol, AC: 4-acetyl-1-methylcyclohexene, CV: carveol, CN: carvone.....	132
Fig. 5.3	The effect of amount H ₂ O ₂ concentration on the oxidation of limonene. Reaction condition: 0.30 g catalyst, 4 h of reaction, 80 °C. LG: limonene glycol, AC: 4-acetyl-1-methylcyclohexene, CV: carveol, CN: carvone.....	133
Fig. 5.4	The effect of temperature on the oxidation of limonene. Reaction condition: 0.30 g catalyst, Time: 4 h. Molar ratio of Limonene: H ₂ O ₂ = 1:1. LG: limonene glycol, AC: 4-acetyl-1-methylcyclohexene, CV: carveol, CN: carvone.	134
Fig. 5.5	Effect of O ₂ ligand used as a homogeneous catalyst versus the heterogeneous RHACO ₂ catalyst (Reaction condition: 0.30 g catalyst (both homogenous and heterogeneous), 4 h, temperature 110 °C, molar ratio of limonene: H ₂ O ₂ = 1:1 Note: The use of 0.3 g O ₂ in this experiment is very high compared to the actual amount of O ₂ present in RHACO ₂ .	136
Fig. 5.6	Limonene conversion (%) for reusability test of oxidation of limonene.....	137
Fig. 5.7	The XRD spectra of used RHACO ₂	138
Fig. 5.8	The TEM micrograph of used RHACO ₂ at different magnification ca. (a) at 100 k and (b) 120 k.....	138
Fig. 5.9	Conversion of limonene versus reaction time with 0.30 g	

	catalyst, and 1:1 molar ratio at a reaction temperature of 80 °C.....	142
Fig. 5.10	The effect of catalyst amount on the oxidation of limonene. Reaction condition: molar ratio of limonene: H ₂ O ₂ = 1:1, 5 h of reaction, 80 °C. LG: limonene glycol, AC: 4-acetyl-1-methylcyclohexene, CV: carveol, CN: carvone.....	143
Fig. 5.11	The effect of amount H ₂ O ₂ concentration on the oxidation of limonene. Reaction condition: 0.35 g catalyst, 5 h of reaction, 80 °C. LG: limonene glycol, AC: 4-acetyl-1-methylcyclohexene, CV: carveol, CN: carvone.....	145
Fig. 5.12	The effect of temperature on the oxidation of limonene. Reaction condition: 0.35 g catalyst, Time: 5 h. Molar ratio of Limonene: H ₂ O ₂ = 1:1. LG:limonene glycol, AC: 4-acetyl-1-methylcyclohexene, CV: carveol, CN:carvone...	146
Fig. 5.13	Effect of P1 ligand used as a homogeneous catalyst versus the heterogeneous RHACP1 catalyst.....	147
Fig. 5.14	Limonene conversion (%) for reusability test of oxidation of limonene.....	149
Fig. 5.15	The XRD spectra of used RHACP1.....	149
Fig. 5.16	The TEM micrograph of RHACP1 at different magnification ca. (a) at 100 k and (b) 120 k.....	150
Fig. 5.17	Conversion of limonene versus reaction time with 0.30 g catalyst, and 1:1 molar ratio at a reaction temperature of 80 °C.....	153
Fig. 5.18	The effect of catalyst amount on the oxidation of limonene.	

	Reaction condition: molar ratio of limonene: H_2O_2 = 1:1, 7 h of reaction, 80 °C. LG: limonene glycol, AC: 4-acetyl-1-methylcyclohexene, CV: carveol, CN: carvone	154
Fig. 5.19	The effect of amount H_2O_2 concentration on the oxidation of limonene. Reaction condition: 0.35 g catalyst, 7 h of reaction, 80 °C. LG: limonene glycol, AC: 4-acetyl-1-methylcyclohexene, CV: carveol, CN: carvone.....	156
Fig. 5.20	The effect of temperature on the oxidation of limonene. Reaction condition: 0.35 g catalyst, Time: 7 h. Molar ratio of Limonene: H_2O_2 = 1:3. LG: limonene glycol, AC: 4-acetyl-1-methylcyclohexene, CV: carveol, CN: carvone.....	157
Fig. 5.21	Effect of P2 ligand used as a homogeneous catalyst versus the heterogeneous RHACP2 catalyst.....	158
Fig. 5.22	Limonene conversion (%) for reusability test of oxidation of limonene.....	160
Fig. 5.23	The XRD spectra of used RHACP2.....	160
Fig. 5.24	The TEM micrograph of RHACP2 at different magnification ca. (a) at 100 k and (b) 200 k.....	161
Fig. 6.1	The EDX analysis of RHACP1Fe.....	166
Fig. 6.2	(a): The nitrogen adsorption /desorption isotherms of RHACP1Fe (b) The corresponding pore size distribution...	167
Fig. 6.3	(a) The XRD spectra of RHACCl. (b)The XRD spectra of RHACP1Fe.....	169

Fig. 6.4	The FTIR spectra of RHACP1Fe.....	170
Fig. 6.5	The ^{29}Si MAS NMR solid-state spectrum of RHACP1Fe. The chemical shifts of T^2 , T^3 , Q^3 and Q^4 are observed.....	171
Fig. 6.6	The possible structures for RHACP1Fe as suggested by MAS NMR and FTIR. (a) T_3 - three siloxane bonds to silicon, (b) T_2 -two siloxane bonds to silicon.....	172
Fig. 6.7	The solid state ^{13}C MAS NMR spectra for RHACP1Fe at 5 KHz. It shows C1, C2 and C3 carbon.....	173
Fig. 6.8	The SEM images of RHACP1Fe at ca. (a) 3 k magnification, (b) 10 k magnification, showing the rod like structure arrangements.....	173
Fig. 6.9	The TEM images of RHACP1Fe at (a) 100 k (b) 200 k magnification showing the irregular pores arrangements.....	174
Fig. 6.10	Thermogravimetric analysis of RHACP1Fe.....	175
Fig. 6.11	Conversion of limonene versus reaction time with 0.30 g catalyst, and 1:1molar ratio at a reaction temperature of 80 °C.....	177
Fig. 6.12	The effect of catalyst mass on the oxidation of limonene. Reaction condition: molar ratio of limonene: H_2O_2 =1:1, 5h of reaction, 80 °C. LG: limonene glycol, AC: 4-acetyl-1- methylcyclohexene, CV: carveol, CN: carvone.....	178
Fig. 6.13	The effect of amount H_2O_2 concentration on the oxidation of limonene.Reaction condition: 0.30 g catalyst, 5 h of	

	reaction, 80 °C. LG: limonene glycol, AC: 4-acetyl-1-methylcyclohexene, CV: carveol, CN: carvone.....	179
Fig. 6.14	The effect of temperature on the oxidation of limonene. Reaction condition: 0.30 g catalyst, Time: 5 h. Molar ratio of Limonene: H ₂ O ₂ = 1:1. LG: limonene glycol, AC: 4-acetyl-1-methylcyclohexene, CV: carveol, CN: carvone.	180
Fig. 6.15	Limonene conversion (%) for reusability test of oxidation of limonene.....	182
Fig. 6.16	The effect of temperature on the oxidation of limonene.....	183
Fig. 6.17	The XRD spectra of used RHACP1Fe.....	184
Fig. 6.18	The TEM micrograph of reused RHACP1Fe at different magnification ca. (a) at 100 k and (b) 120 k.....	184

LIST OF TABLES

	Page
Table 1.1 Classification of dispersed silica system according to Douglas et al., (1995).....	3
Table 1.2 Several Literature Review of Thiourea Derivatives in Catalysis.....	16
Table 1.3 Several Literature Review of limonene oxidation.....	23
Table 2.1 Chemicals used in the analysis.....	30
Table 2.2 The GC and GC–MS condition is used for identification products.....	47
Table 3.1 Crystal data, data collection and structure refinement parameters of 2-methyl- <i>N</i> -[(2-pyridine-2-yl-ethyl) carbamothiol]benzamide.....	51
Table 3.2 Selected bond lengths (Å) and angles (°) for 2-methyl- <i>N</i> -[(2-pyridine-2-yl-ethyl)carbamothiol]benzamide.....	52
Table 3.3 Hydrogen bond geometry (Å, °). Cg ² is the centroid of the C1–C6 ring.....	53
Table 3.4 The splitting pattern, chemical shifts and J coupling of protons in 2-methyl- <i>N</i> -[(2-pyridine-2-yl-ethyl) carbamothioyl]benzamide.....	56
Table 3.5 The elemental analysis of 2-methyl- <i>N</i> -[(2-pyridine-2-yl-ethyl)carbamothioyl]benzamide.....	58
Table 3.6 Crystal data, data collection and structure refinement	

	parameters of 4-methyl- <i>N</i> -[(4-methylpyridin- 2-yl) carbamothioyl]benzamide.....	62
Table 3.7	Selected bond lengths (Å) and angles (°) for 4-methyl- <i>N</i> -[(4-methylpyridin-2-yl)carbamothioyl]benzamide.....	63
Table 3.8	Hydrogen bond geometry (Å, °) of 2-methyl- <i>N</i> -[(2-pyridine -2-yl-ethyl)carbamothioyl]benzamide.....	64
Table 3.9	The splitting pattern, chemical shift and J coupling of protons for 4-methyl- <i>N</i> -[(4-methylpyridine-2-yl)carbamothioyl]benzamide	66
Table 3.10	The elemental analysis of 4-methyl- <i>N</i> -[(4-methylpyridin -2-yl)carbamothioyl]benzamide.....	70
Table 3.11	Crystal data, data and structure refinement parameters of 4-methyl- <i>N</i> -[(2-pyridine-2-yl-ethyl)carbamothioyl] benzamide.....	73
Table 3.12	Hydrogen bond distances and bond angles of 4-methyl- <i>N</i> -[(2-pyridine-2-yl-ethyl)carbamothioyl]benzamide.....	74
Table 3.13	Selected bond lengths (Å) and bond angles (°) of 4-methyl - <i>N</i> -[(2-pyridine-2-yl-ethyl)carbamothioyl]benzamide.....	74
Table 3.14	The splitting pattern, chemical shifts and J coupling of protons in 4-methyl- <i>N</i> -[(2-pyridine-2 -yl-ethyl)carbamothi- oyl]benzamide... ..	78
Table 3.15	The elemental analysis of 4- methyl- <i>N</i> -[(2-pyridine-2-yl- ethyl)carbamothiol]benzamide.....	83

Table 3.16	The splitting pattern, chemical shift and J coupling of protons for 4-methyl- <i>N</i> -[(4-methylpyridine-2-yl) carbamothiolbenzamide.....	85
Table 3.17	The elemental analysis of [Fe(P1)]Cl.....	89
Table 4.1	The physical parameters obtained for RHACO2. The C, H and N content determined by combination of elemental and EDX analysis. The average values obtained from EDX analysis for RHACO2.....	100
Table 5.1	The physical parameters obtained for RHACP1 and RHACCl. The percentage of each element determined by a combination of elemental and EDX analysis. The average values obtained from EDX analysis for RHACP1.....	126
Table 5.2	The surface properties of RHACCl and RHACP1.....	127
Table 6.1	The physical parameters obtained for RHACP2. The C, H and N content determined by elemental analysis. The C, H, N, S, O, Si and Cl content determined by EDX analysis for RHACP2.....	148
Table 6.2	The surface properties of RHACCl and RHACP2.....	150
Table 6.7	Summary of the catalytic study for three catalysts.....	171
Table 7.1	The physical parameters obtained for RHACP1Fe. The C, H and N content determined by combination of elemental and EDX analysis. The average values obtained from EDX analysis for RHACP1Fe. The result of BET analysis was also shown.....	175

Table 7.2 Leaching test of RHACP1Fe..... 190

LIST OF SCHEMES

	Page
Scheme 2.1 The synthesis of 2-methyl- <i>N</i> -[(2-pyridine-2-yl-ethyl) carbamothioyl]benzamide.....	39
Scheme 2.2 The possible chemical equation of 4-methyl- <i>N</i> -[(4-methyl pyridine-2-yl)carbamothioyl]benzamide.....	40
Scheme 2.3 The synthesis of 4-methyl- <i>N</i> -[(2-pyridine-2-yl-ethyl) carbamothioyl]benzamide.....	41
Scheme 2.4 The possible chemical equation of [Fe(P1)]Cl.....	42
Scheme 2.5 Functionalization of RHA with CPTES.....	44
Scheme 2.6 The reaction sequence and the possible structure for RHACO2.....	45
Scheme 2.7 The postulated structures of (a) RHACP1 and (b) RHACP2 and (c) RHACP1Fe showing the bonding connections of the organic ligands.....	46
Scheme 4.1 The reaction sequence and the possible structures for RHACO2 as suggested by ¹³ C MAS NMR and FT-IR. The approximate times taken for the completion of the experimental processes are also shown.....	99
Scheme 4.2 The reaction scheme showing all the possible products in the oxidation of limonene.....	112
Scheme 4.3 The proposed mechanism for the oxidation of limonene by RHACO2 Only the catalytic active site of S and O are	

	shown for clarity.....	122
Scheme 5.1	The reaction scheme between P1 and RHACCl and the potential structure for RHACP1 as suggested by ^{13}C MAS NMR and FT-IR. The approximate times taken for the completion of the experimental processes are also shown..	124
Scheme 5.2	The reaction scheme showing all the possible products in the oxidation of limonene.....	136
Scheme 6.1	Immobilization reaction scheme of P2 onto RHACC1 to form RHACP2. The approximate time taken for the completion of the experimental process is shown.....	147
Scheme 6.2	The reaction scheme showing all the possible products in the oxidation of limonene.....	160
Scheme 7.1	The reaction sequence for the synthesis of RHACP1Fe. The possible structures of the catalyst are represented from MAS NMR and FT-IR spectra studies. The carbons of the propyl chain (C_1 , C_2 and C_3) were identified by their ^{13}C MAS NMR spectrum.....	173
Scheme 7.2	Oxidation of limonene over RHACP1Fe as a catalyst.....	184
Scheme 7.3	The proposed mechanism for the oxidation of limonene by RHACP1Fe.....	194

LIST OF ABBREVIATIONS

A	Frequency factor
AAPTS	<i>N</i> -(2-aminoethyl)-3-aminopropyltrimethoxysilane
APTES-SNPs	Aminopropyltriethoxysilane-Silica nanoparticles
CHN	Carbon, Hydrogen and Nitrogen Analysis
CP/MAS NMR	Cross Polarisation/Magic Angle-Spinning Nuclear Magnetic Resonance
CPTES	3-chloropropyltriethoxysilane
BET	Brunauer-Elmmet-Teller
BTU	Benzoylthiourea
BTU-SNPs	Benzoylthiourea-Silica nanoparticles
ca.	Calculated
CN	Carvone
CV	Carveol
d	doublet
DCM	Di-chloromethane
DETA	diethylenetriamine
DMF	Dimethyl formamide
DMSO	Dimethyl sulfoxide
EDA	ethylenediamine
EDX	Energy Dispersive X-Ray
ELDIOL	Ethylene Diol
Et ₃ N	Tri-ethylamine
EPME	Epoxy-p-menta-1-ene
FAO	Food Agricultural Organisation
Fe(II)-BTU-SNPs	Iron(benzoylthiourea)silica nanoparticles
FID	Flame Ionisation Detector
FT-IR	Fourier Transform Infra-Red Spectroscopy
FTU	FuroylThiourea
GC	Gas chromatography
GC-MS	Gas chromatography Mass Spectroscopy
h	Hour

Hz	Hertz (Unit of Frequency Equal to One Cycle Per Second)
IUPAC	The International Union of Pure and Applied Chemistry
K	Kelvin (absolute temperature Unit)
LO	Limonene Epoxide
LG	Limonene Glycol
LNON	Limonenone
MCM-41	Mobil Crystalline Material Number 41
min	Minute
mL	Mililiters
Mol	Mole
MSNs	Mesoporous silica nanoparticles
O2	2-methyl- <i>N</i> -[(2-pyridine-2-yl-ethyl) carbamothioyl]benzamide
P1	4-methyl- <i>N</i> -[(4-methylpyridin-2-yl)carbamothioyl]benzami- de
P2	4-methyl- <i>N</i> -[(2-pyridine-2-yl-ethyl)carbamothiol]benzamide
P/Po	Relative Pressure
pg.	Page
PA	Perrilylaldehyde
PO	Perillyl alcohol
PS	Post Synthetis
Ppm	Part per Million (Chemical Shift Unit)
PS-II	Post Synthetis Ion-Imprinting
P-C	<i>Para</i> -Cyamine
PCS	sodium percarbonate
PBS	sodium perborate
PMO	Periodic mesoporous organosilica
Q ²	Silicon atom bearing two hydroxyl groups and bonded to two silicon atoms via oxygen bond
Q ³	Silicon atom bearing one hydroxyl groups and bonded to three silicon atoms via oxygen bond
Q ⁴	Silicon atom not bonded to any hydroxyl groups and bonded to four other silicon atoms via oxygen bond

R	Alkyl group
RH	Rice Husk
RHA	Rice Husk Ash
RHACO2	Rice Husk Ash incorporated with O2 ligand
RHACP2	Rice Husk Ash incorporated with P2 ligand
RHACP1	Rice Husk Ash incorporated with P1 ligand
RHACP1Fe	Rice Husk Ash incorporated with metal complex of P1
RMM	Rice Market Monitor
r.t.	Room Temperature
SBA-15	Santa Barbara Amorphous Material Number 15
SDA	Structure Directing Agent
SEM	Scanning Electron Microscopy
Si-OH	Silanol
Si-O-Si	Siloxane
SG-PrCl	[Chloropropyl] silica gel
SG-Pr-THIO	[3-(thiourea)-propyl] silica gel
SG-Pr-THIO-Mo	[3-(thiourea)-propyl] silica gel with Molybdenum
SNPs	Silica nanoparticles
T	Absolute Temperature
TETA	triethylenetetramine
T ¹	Silicon Atom Bearing Two Hydroxyl Groups
T ²	Silicon Atom Bearing One Hydroxyl Groups
T ³	Silicon Atom not Bonded to any Hydroxyl Group
TS	Titanium silicate
TBHP	tert-butyl hydroperoxide
TEM	Transmission Electron Microscopy
TUD	Thiourea Dioxide
TEOS	Tetraethyl orthosilicate
TMOS	Tetramethyl orthosilicate
TUD	Thiourea dioxide
UHP	urea-hydrogen peroxide
XRD	Powder X-ray Diffraction
¹ H NMR	Hydrogen-1 Nuclear Magnetic Resonance

^{13}C NMR

Carbon-13 Nuclear Magnetic Resonance

^{29}Si NMR

Silicon-29 Nuclear Magnetic Resonance

LIST OF SYMBOLS

Å	Angstrom
C	Celsius (Centigrade Temperature Scale)
d	doublet
d ₆	Deuterated Solvent
% T	Transmittance
s	Singlet
t	Triplet
λ	Wavelength
δ	Chemical Shift
°C	Degree Celsius (Centigrade Temperature Scale)
k	Kilo (1000)
<i>M</i>	Molar amount of Grafted
<i>N</i>	Surface Coverage

**PENGHETEROGENAN KOMPLEKS FERUM-KARBONIL TIOUREA KE
ATAS SEKAM PADI DAN AKTIVITI PENGOKSIDAAN LIMONIN
DENGAN HIDROGEN PEROKSIDA**

ABSTRAK

Tiga ligan tiourea yang baru 2-metil-*N*-[(2-piridina-2-il-etil)karbamotiol]benzamida, O2; 4-metil-*N*-[(4-metilpiridina-2-il)karbamotiol]benzamida, P1; dan 4-metil-*N*-[(2-piridina-2-il-etil)karbamotiol]benzamida, P2 telah disintesis dan dicirikan melalui pelbagai teknik spektral dan analitikal seperti NMR (^1H and ^{13}C), spektroskopi FTIR dan analisis unsur. Struktur molekul untuk tiga jenis terbitan tiourea telah dikenalpasti melalui teknik pembelauan sinaran-X kristal tunggal. Ligan tersebut telah dimodifikasikan dengan menggunakan 3-kloropropiltriethoxysilina (CPTES) sebagai ejen pencantuman terhadap abu sekam padi (RHA). Mangkin yang telah dihasilkan telah ditetapkan sebagai RHACO2, RHACP1 dan RHACP2. Pencirian spektroskopik membuktikan pencantuman ligan organik pada rangka silika. Analisis ^{29}Si MAS NMR pada RHACP1 dan RHACP2 menunjukkan kewujudan pusat silikon T^1 , T^2 , Q^2 dan Q^3 manakala pusat silikon T^2 , T^3 , Q^3 dan Q^4 wujud pada RHACO2. Spektrum ^{13}C MAS NMR menunjukkan anjakan kimia pada moiety $-\text{CH}_2\text{CH}_2\text{CH}_2-$. RHACO2 memiliki anjakan kimia pada 24.97, 41.72 dan 62.82 ppm manakala RHACP1 dan RHACP2 memiliki anjakan kimia masing-masing pada 23.52, 40.17, 60.40 ppm, 26.68, 47.86 dan 63.02 ppm. Spektrum ^{13}C MAS NMR menunjukkan kesemua mangkin mempunyai siri anjakan kimia yang konsisten dengan kehadiran gelang aromatik benzena dan juga piridin. Dalam kajian ini, mangkin - mangkin ini telah digunakan dalam pengoksidaan limonin. Produk utama yang terhasil ialah epoksida limonin dengan produk

sampingan. Berdasarkan kepada parameter optimum, susunan kereaktifan pemangkin ditemui untuk menjadi seperti urutan berikut: $RHACP1 > RHACO2 > RHACP2$. Kesan sterik yang lebih tinggi pada P2 seolah-olah memberikan perubahan kereaktifan yang rendah pada RHACP2 berbanding RHACP1. P1 ligan telah dikomplek dengan ferum (II). Potensi untuk menggunakan ferum dalam proses kimia ini disebabkan oleh efisiensi kos dan mesra alam. Kompleks logam yang terhasil telah dipegun terhadap RHA silika untuk menghasilkan pemangkin baru, RHACP1Fe. Ia telah dicirikan dan digunakan dalam pengoksidaan limonin. Produk utama adalah epoksida limonin manakala produk sampingan terhad hanya kepada karvon dan karviol. Didapati bahawa penggabungan ferum (II) telah menyebabkan penurunan drastik jumlah produk sampingan (karvon dan karviol). Hasil LO didapati sebanyak 46.23 % dengan 69.00% daripada penukaran limonin dan 67.00 % daripada pemilihan LO. Mangkin ini boleh didapati semula melalui penapisan dan digunakan semula untuk sekurang-kurangnya tiga kali tanpa kehilangan aktiviti pemangkin ketara. Lima et. al., (2006) menghasilkan kompleks logam (salen) dan digunakan sebagai pemangkin pengoksidaan limonena dengan nisbah molar yang sama Limonene: H_2O_2 dalam asetoniril sebagai pelarut pada 80 °C. Walaupun tindak balas itu berlaku pada suhu yang lebih rendah, dan menghasilkan 45.1 % limonene epoksida, bagaimanapun, kelemahannya adalah cabaran untuk memisahkan pemangkin dari campuran tindak balas, sifat pemangkin yang mengakis dan sifatnya yang berbahaya. Oleh itu, penanda aras aktiviti pemangkin ini telah digunakan untuk disiasat. Maka, pemangkin heterogen yang mempunyai ligan organik dengan memuat atau mencantumkan sokongan padu dari abu sekam padi telah digunakan.

**THE HETEROGENATION OF IRON-CARBONYL THIOUREA COMPLEX
ONTO RICE HUSK SILICA AND ITS CATALYTIC OXIDATION OF
LIMONENE WITH HYDROGEN PEROXIDE**

ABSTRACT

Three new thiourea ligands (2-methyl-*N*-[(2-pyridine-2-yl-ethyl)carbamothioyl]benzamide, O2; 4-methyl-*N*-[(4-methylpyridin-2-yl) carbamothioyl]benzamide, P1; and 4-methyl-*N*-[(2-pyridine-2-yl-ethyl)carbamothioyl]benzamide, P2) were synthesized and characterized by various spectroscopic and analytical techniques viz., NMR (¹H and ¹³C), FTIR and elemental analysis. Molecular structure of three thiourea derivatives were established through single crystal X-ray diffraction technique. The ligands O2, P1 and P2 were functionalized using chloropropyltriethoxysilane (CPTES) as the anchoring agent onto rice husk ash (RHA). The resultant catalysts were designated as RHACO2, RHACP1 and RHACP2. Spectroscopic characterisation confirmed the successful immobilization of the organic ligands on the silica framework. The ²⁹Si MAS NMR of RHACP1 and RHACP2 showed the presence of T¹, T², Q² and Q³ while the T², T³, Q³ and Q⁴ were present in RHACO2. The ¹³C MAS NMR showed the chemical shifts of –CH₂CH₂CH₂– moiety. RHACO2 had chemical shifts at 24.97, 41.72 and 62.82 ppm while RHACP1 and RHACP2 had chemical shifts at 23.52, 40.17, 60.40 ppm, 26.68, 47.86 and 63.02 ppm respectively. The ¹³C MAS NMR demonstrated that all the catalysts have a series of chemical shifts which is compatible with the existence of pyridine ring and aromatic benzene ring. In this study, these catalysts have been used in the oxidation of limonene. The main product obtained was limonene epoxide (LO) with many side products. Limonene epoxide which is the principle item would be

vital as intermediates for organic synthesis for various items such as in pharmaceuticals products, food additives, and scents. Based on the optimum parameters, the order of the catalyst's reactivity was found to be: RHACP1 > RHACO2 > RHACP2. The higher steric effect of P2 seems to be change of the low reactivity of RHACP2 compared to RHACP1. The yield of LO obtained for RHACO2, RHACP1 and RHACP2 were 40.02 %, 63.20 % and 25.65 % respectively. P1 ligand was complexed with iron (II). The potential to utilize iron in this chemical processes are due to its cost-efficient and ecological-friendly. The resulting metal complex was immobilized onto RHA silica to produce a new catalyst, RHACP1Fe. It was characterized and used in the oxidation of limonene. The main product was limonene epoxide while the side products were limited only to carvone and carveol. It was found that the incorporation of the iron (II) resulted in the drastic reduction of the number of side products (carvone and carveol). The yield of LO was found to be 46.23 % with 69.00 % of limonene conversion and 67.00 % of LO selectivity. Filtration can be used to efficiently recover these catalysts. These catalysts are reused for a minimum of three times without considerable loss in its catalytic action. Lima et. al., (2006) produced metal (salen) complex and used as a catalyst in oxidation of limonene with same molar ratio of Limonene: H₂O₂ in Acetonitrile as a solvents at 80 °C. Eventhough the reaction was took place in at lower temperature, and produced 45.1 % of limonene epoxide, however, the drawback is the challenge to separate the catalysts from the reaction mixture, the corrosive nature of the catalyst and their hazardous properties. Thus this benchmark of catalytic activity has been used to be investigated. Therefore, heterogeneous catalyst possessing organic ligands by loading or grafting onto a solid support from rice husk ash was used.

CHAPTER 1

INTRODUCTION

1.1 General Introduction

It has been discovered that the production of fine chemicals by using homogeneous catalyst has many disadvantages. The disadvantages include non-reusability of the catalyst, the problem of dissociation (Ghiaci et al., 2010) inefficient in terms of separation and recovery process and in most cases contribute to environmental hazards. Therefore, the development of efficient heterogeneous catalyst is being explored to control this adverse situation in the industry (Hadi et al., 2015). Catalyst is a substance that speeds up the chemical reaction without itself being spent (Battegazore et al., 2014). There is a decrease in the activation energy which permits the creation of an alternative pathway for the reaction to happen. Silica is a catalysis supporter that is most commonly studied. It possesses strong chemical resistance and high-temperature resistance.

Two primary categories of catalysts are homogenous and heterogeneous. Despite that, homogenous reactions have several disadvantages in terms of recovery and reuse. Besides that, it is costly. On the other hand, heterogeneous catalyst presents many benefits such as ease of recovery and can be reused. Therefore, it is more economical and cost-efficient as compared to homogeneous catalyst (Nur et al., 2006).

1.2 Silica

Silica is made up of oxygen and silicon. The qualities of silica are high melting point, hard, and chemically inert. The qualities are determined based on the strength of the bonds between the atoms (Baccile et al., 2009). Despite crystalline

silica being one of the most abundant material in the earth's crust, the utilization is constrained since silica has low reactivity (Chen et al., 2015). Crystalline silicon is distinct to amorphous silicon. This is because the SiO_2 stoichiometric in amorphous silicon dioxide is devoid of crystalline structure as determined by the X-ray diffraction spectra. The primary composition on the silica's surface is siloxane and silanol. Silica becomes chemically efficacious when the surface was appropriately modified. The presence of organic modifier enables surface reaction to occur by forming new bonds, i.e. $\equiv\text{Si}-\text{O}-\text{C}\equiv$, $\equiv\text{Si}-\text{C}\equiv$, $\equiv\text{Si}-\text{N}=\text{}$. Silica is usually porous. The porosity of silica can be formed by the random condensation of sodium silicate and the pore space made up of interstices between particles during compaction.

The importance of silica as heterogeneous support in catalysis has seen an ascending growth in the past decade. The versatility of functionalization techniques of mesoporous materials along with the ability to readily separate from the products upon reaction completion has allowed for continuous innovation in its use in catalysis (Yu, 2013). Silica can be prepared easily from the precursors such as tetraethylorthosilicate (TEOS) and tetramethylorthosilicate (TMOS) (Nabavi and Alizadeh, 2014); (Han et al., 2016), sodium metasilicate and colloidal silica. However, these well-known precursors are toxic, expensive and hazardous (Nakashima et al., 1998). Naturally occurring silica from biomass such as paddy plants and their waste can provide an alternative as it is cheaper and a safer source of silica. The pore space is comprised of crevices between the particles which was promotes the porosity of the silica. The size of the pore measure of silica does significantly influence particular application, for example, adsorption of large molecule from effluent, separation of proteins and catalysis (Liu et al., 2015). Solid silica can be distributed in liquid or gaseous medium.

Table 1.1 demonstrates that silica can exist in a separated system with various types of amorphous.

Table 1.1: Classification of dispersed silica system according to Douglas et al., (1995).

Silica sols-colloidal silica	Sols formed from pH adjustment with acid which undergo polycondensation and polymerisation occur to grow into colloidal particles. Stable dispersions/sols of discrete particles of amorphous silica.
Silica hydrogel	Dispersed silica particles aggregate forming colloidal silica particles which are linked together. Silica gel, in which the pores orifice are filled with the corresponding liquid (water).
Silica xerogels	Dehydration process of hydrogels that leads to partial collapse of globular structure leading to xerogels. A gel from which the liquid medium has been removed, resulting in a compressed structure and a reduced porosity.
Silica aerogels	High-temperature hydrolysis of silica compounds to produce spherical amorphous particles. The liquid has been removed in such a way as to prevent any collapse or change in the structure as liquid is removed.
Polymeric silica solutions	Partial hydrolysis of alkoxysilanes that results in macromolecular solutions.
Pyrogenic	Silicas made at high temperatures.
Aerosils	Flame hydrolysis products of SiCl_4 ; very pure materials.
Arc silicas	Made by the reduction of high purity sand.
Plasma	Ultra-fine silica powders, made by the direct volatilization of sand in a plasma jet.

1.2.1 Silica in rice husk (RH) and rice husk ash (RHA)

Paddy plant is a place where silica can be found. Food and Agricultural Organization (FAO) of United Nations have presented in a report that Asia was the region that produces the largest amount of world rice production with an astounding

92 % while Asia produces 90 % of production for global rice consumption. Thus forecast paddy production has increased in 2016 by 1.3 million tonnes to 746.8 million tonnes (Pourbafrani et al., 2014). Henceforth, rice has been considered a staple sustenance for Asian nations. One ton of husk is created for each five tons of rice that was harvested. It is approximately 1.2×10^8 tons of RHs for every year globally (Liu et al., 2013).

The large amount of RH from the rice milling process has resulted in disposal problems. In addition, the rusk rice is being ignored nowadays. Thus it is becomes more worthwhile as it can be converted into more useful product (Yalcin et al. 2001). RH is comprised of 32 % of cellulose, 15 % of ash and 21 % of lignin. The mineral ash comprises of 2.11 % of K_2O , 96.34 % of SiO_2 , 0.20 % of Fe_2O_3 , 0.45 % of MgO , 30.41 % of CaO and 0.08 % of MnO_2 (Woranan et al., 2007). The original source of RHA is from RH burning. The burning process removes lignin and cellulose and leaves just silica ash (Adam et al., 2012a). Subsequently, in this current research, rice husk was calcined to attain white ash or known as RHA as depicted in Fig. 1.1.

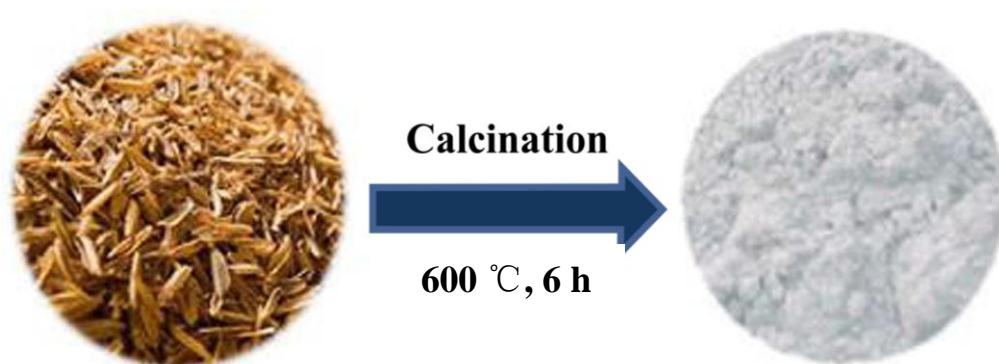


Fig. 1.1: The conversion of rice husk to rice husk ash (RHA).

1.2.2 The silanol and siloxane bonds in RHA

There are three types of silanol and siloxane bonds within the silica matrix.

Fig. 1.2 shows the three types of bonds in silica. First, the geminal (two hydroxyl

group attached to the silicon atom, $=\text{Si}(\text{OH})_2$). Second, isolated group (a single hydroxyl group attached to the same silicon atom, $(=\text{SiOH})$ as shown in Fig. 1.2. The last group is, the vicinal silanol where the isolated silanol are in adjacent to the silicon atoms which are linked by intramolecular hydrogen bond (Yang et al., 2010). As the surface area of RHA is large, it contains abundant Si-OH groups for silylating agents to anchor easily. Thus, the free hydroxyl group is able to displace the alkoxy groups onto silane to create covalent bonds of Si-O-Si. This is the primary reason why silanol groups play a crucial role in the modification of silica surface with the use alkyl silane (Dash et al., 2008). When the temperature increase, the silanol groups would undergo the dehydration on the silica surface which results in the formation of siloxane bonds (Peng et al., 2012). Antonio et al. (2001) found that silylating agents are chemically reactive towards the free silanol groups.

The three siloxane bonds are discerned as (i) Q^2 – silicon atom bearing two hydroxyl groups and bonded to two silicon atoms via oxygen bond, (ii) Q^3 – silicon atom bearing one hydroxyl group and bonded to three silicon atom via oxygen bond and (iii) Q^4 – silicon atom not bonded to any hydroxyl group and bonded to four other silicon atoms via oxygen. ^{29}Si CP/MAS NMR spectrum can be referred to identify these silicon atoms. The superscript number [n] is derived from the general equation, $\text{Q}^n = \text{Si}(\text{OSi})_n(\text{OH})_{4-n}$ by Adam and Batagrawa, (2013) and conforms to the number of $(-\text{O}-\text{Si})$ bond linked to the respective silicon atom.

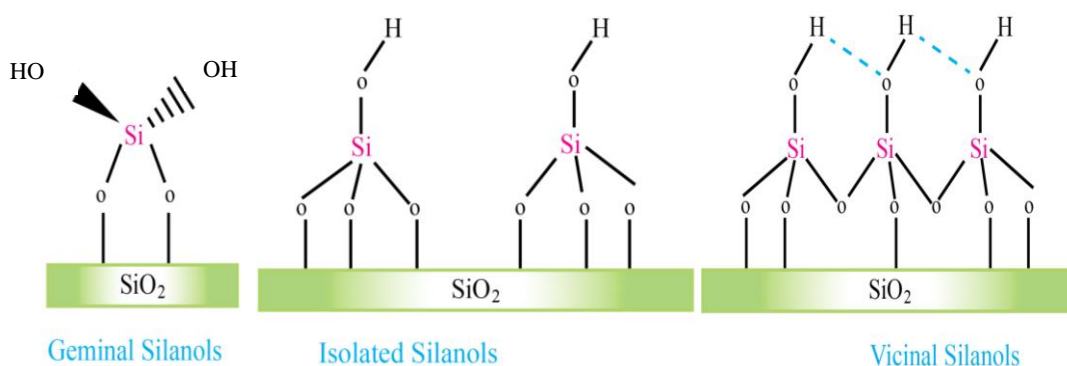


Fig. 1.2: Different forms of silanol groups at the silica surface (Sharma et al., 2015).

The silicon atom of the propyl silane was illustrated in Fig 1.3 which creates a bridge with the silica surface after modification. These silicon atoms can be monitored from the ^{29}Si solid state NMR which give distinct signals depending on the nature of silicon atom's attachment. The NMR signals are identified as (i) T^1 – silicon atom bearing two hydroxyl groups, (ii) T^2 – silicon atom bearing one hydroxyl group and T^3 – silicon atom not bonded to any hydroxyl group.

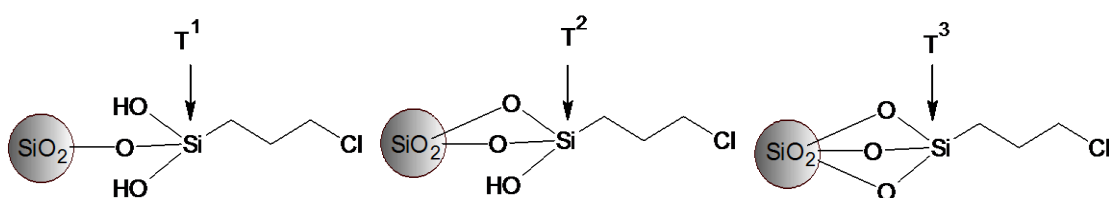


Fig. 1.3: The silica surface with various bridging formation to the silicon of propyl silane. The nature of the T^1 , T^2 and T^3 silicon atoms in the immobilized silica.

1.3. Organically functionalised mesoporous materials

The incorporation of organic onto the silica structure has been attempted by several effort. The fascinating notion for researchers to explore originates from the idea of combining the properties of inorganic and organic construction unit in a single material. Distinctive applications have been studied by utilizing hybrid materials, for example, sensing, optics, separation, microelectronic, and finally as a catalyst (Hoffmann and Froba, 2011). There are three main approaches for the synthesis of porous hybrid materials depending on the organoalkoxysilane units (Fig. 1.4).

1. Grafting approach: grafting refers to the modification of a pre-fabricated mesoporous support by attachment of functional molecules to the surface of the

mesopores. Mesoporous silicates possess surface silanol (Si-OH) groups that act as convenient anchoring points for organic functionalisation. Surface modification with organic groups is most commonly carried out by silylation. The advantage of post-synthetic method is that the mesostructure of the starting silica phase is usually retained, whereas the lining of the walls is accompanied by a reduction in the porosity of the hybrid material.

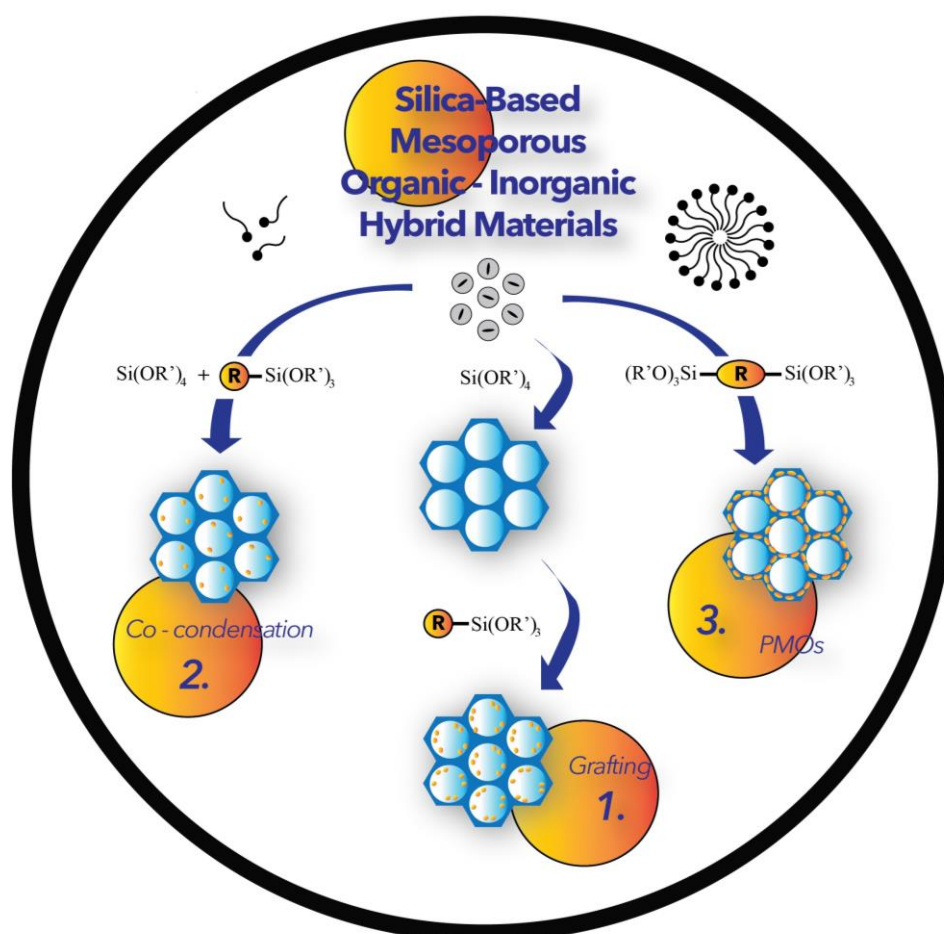


Fig. 1.4: Three synthesis approaches for the synthesis of mesoporous hybrid materials (Hoffman et al., 2006). Where, $\text{Si}(\text{OR}')_4$

2. Co-condensation approach (one-pot synthesis): involves the preparation of mesostructured silica phases by the co-condensation of $[(\text{RO})_4\text{Si}]$; i.e. tetraethyl orthosilicate (TEOS) or tetramethyl orthosilicate (TMOS)] with terminal trialkoxysilanes of the type $(\text{RO})_3\text{SiR}$. A structure directing agent (SDA) is used

to bring about materials with organic residues anchored covalently to the pore walls. The drawbacks are, first, the degree of mesoscopic order of the products decreases with increasing concentration of $(\text{RO})_3\text{SiR}$ in the reaction mixture, which ultimately leads to totally disordered products. Second, an increase in loading of the incorporated organic groups can lead to a reduction in the pore diameter, pore volume and specific surface area.

3. Periodic mesoporous organosilica (PMO) production approach: this was first used in 1999 (Inagaki et al., 1999; Hoffnam and Froba et al., 2011) by hydrolysis and subsequent condensation reactions of the bridged organosilica precursors of the type $(\text{RO})_3\text{Si-R-Si}(\text{OR}')_3$, which had long been known from sol-gel chemistry (Ren et al., 2010).

1.4 Hydrogen bonded urea and hydrogen peroxide

Ortho and *para* benzoylthiourea ligands were selected in this study due to their property to release and accept proton easily. In this work, the ligands synthesised were tailored for oxidation of limonene. This reaction was catalysed at the C=O and C=S active sites of the catalysts. Hydrogen peroxide was used as an oxidising agent. In fact, H_2O_2 is a relatively weak oxidising agent (Clark and Jones, 1999). It can effect oxidations unaided, e.g. it reacts slowly with substrates such as aromatic hydrocarbons and alkanes but for the majority of applications, it requires activation in one way or another.

Basically activation of hydrogen peroxide by transition metal ions is the method of choice. However, the reaction of hydrogen peroxide with organic compounds can, therefore, provide a viable alternative to metal ion activation. There are two solid peroxygens which dominate the area of inorganic hydrogen peroxide

chemistry, namely sodium percarbonate (PCS) and sodium perborate (PBS). It is also worth observing that the urea hydrogen-bonded complex of hydrogen peroxide, known as urea-hydrogen peroxide (UHP) is also an important solid peroxygen which will be discussed here. UHP is represented by the structure in Fig. 1.5.

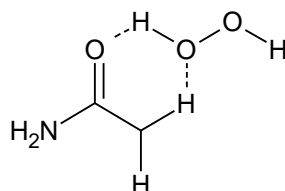


Fig. 1.5: Hydrogen-bonded complex of urea and hydrogen peroxide (UHP).

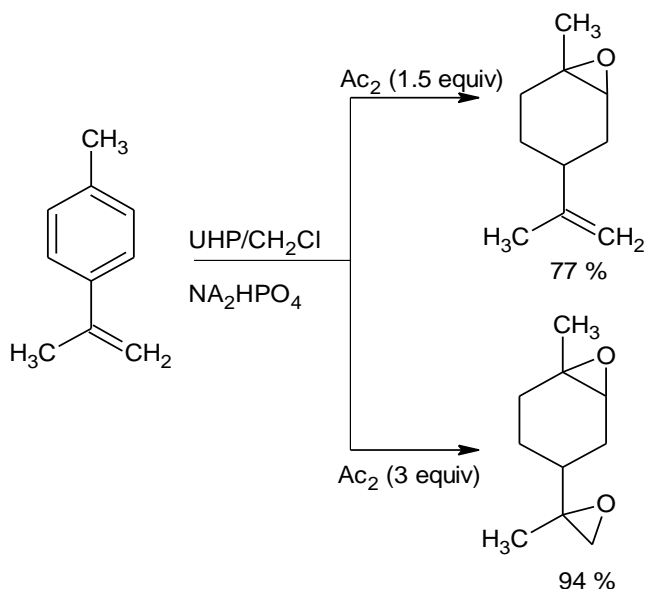


Fig. 1.6: Use of UHP to oxidize an organic compound to industrially useful intermediates.

UHP is readily crystallised from concentrated hydrogen peroxide and urea solution. Since it is anhydrous and essentially a neutral complex, it is a favourable alternative to very highly concentrated hydrogen peroxide (> 85 %) which is difficult to obtain and relatively hazardous. The application of UHP in organic synthesis has been explored and has been verified to be a suitable substitute for concentrated hydrogen peroxide in generating trifluoroperacetic acid from the

anhydride. An example of reactions that utilise UHP to generate peroxyacids in situ is shown in Fig. 1.6 (pg. 9).

1.5 Thiourea

1.5.1 Introduction to thiourea

Thiourea, CSN_2H_4 is an organic compound which contains carbon, nitrogen, sulfur, and hydrogen atoms. In addition, the synonymous name is sulfoarea or thiocarbamide. The structure of thiourea is similar to urea but the oxygen atom in urea is replaced by sulfur. Thus, the property of thiourea and urea is different due to the relative electronegativities of sulfur and oxygen. Fig. 1.7 below shows the general structures of thiourea and urea (Yusof et al., 2010). Fig. 1.8 shows the basic structure of benzoylthiourea derivatives.

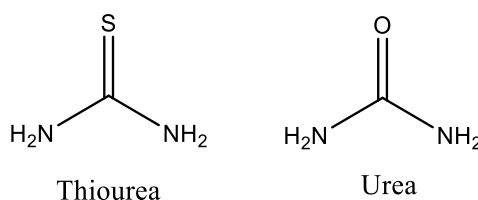
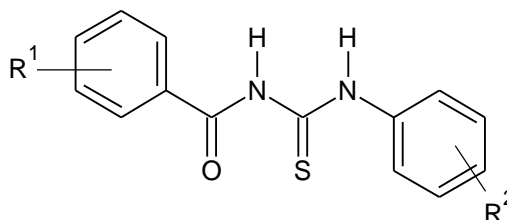


Fig. 1.7: Structure of urea and thiourea.



$\text{R}^1 = \textit{ortho}$ position of methyl, $\text{R}^2 = \textit{ethyl}$ pyridine ; O2

$\text{R}^1 = \textit{para}$ position of methyl, $\text{R}^2 = \textit{methyl}$ pyridine; P1

$\text{R}^1 = \textit{para}$ position of methyl, $\text{R}^2 = \textit{ethyl}$ pyridine: P2

Fig. 1.8: General structure of benzoylthiourea

1.5.2 Thione–thiol tautomerism

Similar to thiosemicarbazones by Haque et al., (2015) thione–thiol tautomerism is plausible for acylthioureas since a thioamide --NH--C=S-- functional group is present, as well as a carbonyl group, which can accept hydrogen-bonding donor groups (Gholivand et al., 2014). In Fig. 1.9 the thione (middle structure) and thiols tautomers are shown. The thione form is strongly preferred, and to the best of our knowledge, there are no reports on compounds showing the thiol form as the most stable tautomer.

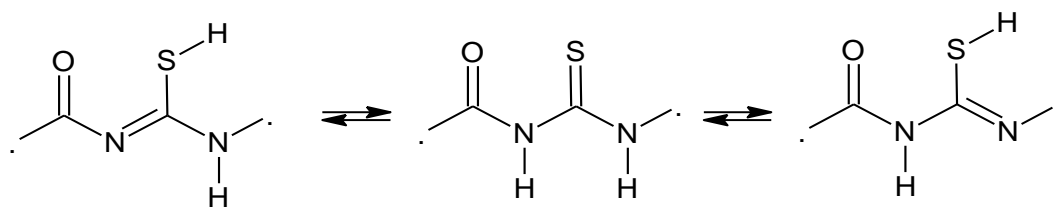


Fig. 1.9: Thione–thiol tautomerism in acylthioureas.

Saeed and coworkers, (2103) reported the infrared spectrum of solid 1-(2-fluorobenzoyl)-3-(4-methoxyphenyl)thiourea, where a weak band appearing at 2438 cm^{-1} could be assigned to the $\nu(\text{S--H})$ stretching mode.

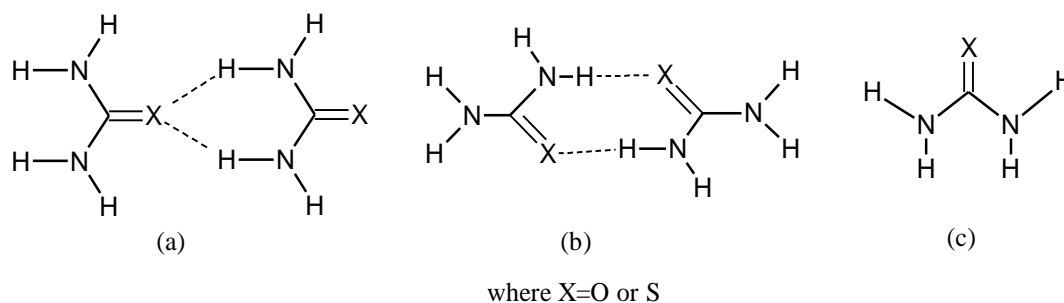


Fig. 1.10: Typical Hydrogen-Bonding Modes of Urea/Thiourea Molecules: (a) Head to-Tail; (b) Shoulder-to-Shoulder; (c) Designation of syn- and anti-Hydrogen Atoms.

A work reported by Saeed et al. (2013), suggested that tautomeric equilibrium exists in 4-(3-benzoylthioureido)-benzoic acid, promoted by an intramolecular proton shift between the thioketo-sulfur and the amine-nitrogen, via

intramolecular hydrogen bonding $\text{N-H}\cdots\text{S}$ or $\text{S-H}\cdots\text{N}$. There are three principal modes of inclusion compounds of urea/thiourea that are stabilized by conventional hydrogen bonds. The classical type of hydrogen bonding having a host lattice constructed from urea/thiourea molecules which is illustrated in Fig. 1.10 (pg 11).

1.5.3 The metal transition complexes of thiourea

An early review of 1-(acyl)-3-substituted thioureas was reported by Beyer et al. (1981) in coordination chemistry particularly about their coordination with some first-row and second-row transition metals. The presence of these hard and soft donor sites offers a huge array of bonding possibilities which were C=O carbonyl and C=S thiocarbonyl. Three coordination mode have been reported so far, monobasic bidentate or chelating mode (O, S), (Sreekanth et al., 2003): (Antoschuk et al., 1999) and neutral bidentate (O, N) modes (Rotondo et al., 2014) (Fig. 1.11). 1-(benzoyl)-3, 3-(di-alkyl) thiourea ligands are able to exhibit neutral monodentate coordination through the S atom as well as the normal monobasic O, S bidentate coordination (Karipcin et al., 2011).

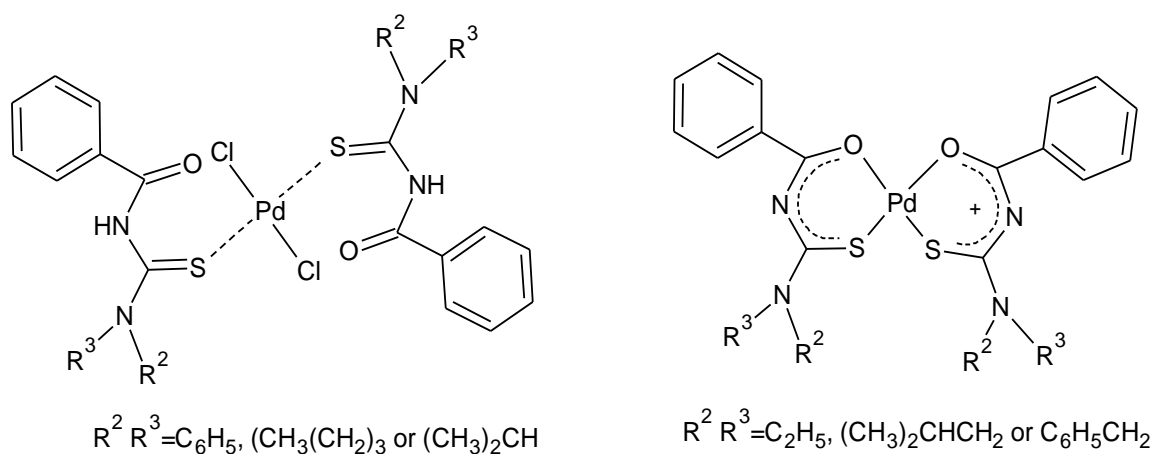


Fig. 1.11: Neutral monodentate through the S atom (left) and monobasic O, S bidentate (right) coordination modes found in Pd(II) complexes of 1-(benzoyl)-3, 3-(di-alkyl) thioureas. Adapted from reference (Karipcin et al., 2011).

1.5.4 Iron

Among the large variety of transition metals which were used as catalysts, iron plays a special role. Dissimilar to harmful metals like osmium, chromium and cadmium, iron is physiologically-accommodating and a ecological friendly metal. The few toxic iron compounds can easily be oxidized or hydrolyzed to harmless iron salts. Iron is the fourth most common element in the earth's crust (after oxygen, silicon and aluminium). It consists of approximately 5.0 % by weight of the Earth's solid surface. The plenitude of iron in the earth's crust renders enables iron to be considered as an inexpensive metal source as compared with those valuable metals which are both costly and destructive to the environment. Its low costs combined with their ecologically benevolent nature offer the likelihood to draw in iron in many fine chemical activities, for example, dihydroxylation of olefins, allylic substitution reactions, cross-coupling of organic halides with organometallic reagents and epoxidation reactions.

1.5.5 Thiourea immobilised silica as a support

Urea and urea-type compounds create viable catalyzing agents when supported onto mesostructures. They are considered as supported organocatalysts which have been used to catalyse organic reactions. Lin and collaeague arranged a series of urea-and thiourea-functionalised MSNs and examined their catalytic examination in the Diels–Alder reaction amongst crotonaldehyde and cyclopentadiene. In this case, the prepared catalysts exhibited a superior catalytic activity towards the Diels–Alder reaction than did homogeneous analogues. They attributed the enhancement in the catalytic activity to a cooperative acid base system. Four urea-and thiourea-supported MSNs were also analyzed and among

them, it was found those containing the solid electron-withdrawing group CF_3 can improve Lewis acidity of these heterogeneous organocatalysts and hence yield the best outcome. Therefore, they form an efficient cooperative catalytic system.

Rostamnia's group simultaneously incorporated APTS [*N*-(2-aminoethyl)-3-aminopropyltrimethoxysilane] with urea on the surface of MSN (Mesoporous Silica Nanoparticles) and investigated it in the aldol reaction. They used a 3-ureido-propyl group as an acid and APTS as a base to perform aldol, Henry and cyanosilylation reactions. (Refer Fig. 1.12).

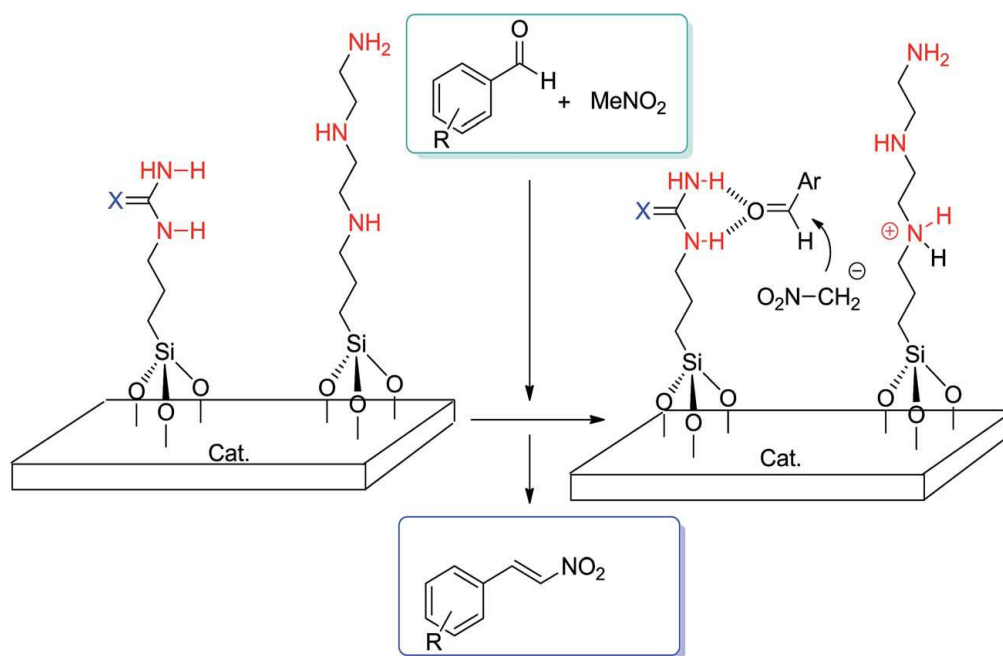


Fig. 1.12: Cooperative catalysis by acid and base bifunctionalized MSN.

There are many reports on the homogenous catalysts of different organic ligand based on thiourea moiety for different types of catalytic oxidation. Thiourea has also been used extensively and commercially used such as herbicides, fungicides and insecticide agent in the agrochemical industries. Other than that, it is being used widely in pharmaceutical industry for potential therapeutic agents as antibacterial, for example, *N*-(4-(hexyloxy)phenyl)-*N'*-(4-methoxybenzoyl)thiourea (Peng et al.,

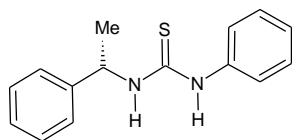
2012). Besides, 1-Benzoyl-3-propylthiourea is an effective adsorbent for removal of mercury ions from aqueous solutions (Yusof et al., 2010). Although these thiourea derivatives have been used in many areas, their application in heterogenous catalysis is comparatively unexplored. A literature review of these different heterogenous catalysts in different area of catalysis is tabulated in Table 1.2. The work embodied in this thesis is the first report detailing the immobilisation of carbonylthiourea moiety onto silica support and used as a catalyst in the oxidation of limonene.

1.5.6 Literature Review of Thiourea Derivatives

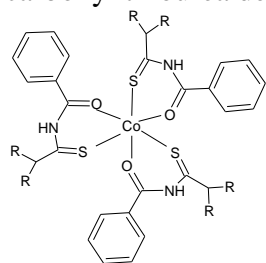
Table 1.2: Several Literature Review of Thiourea Derivatives in Catalysis

Chelating Group	Functionalised silica/ Application	References
Thiosemicarbazide	Separation and selective extraction of palladium (II) from other interfering metal ions	(Mahmoud et al., 2000)
Iminodithiocarbamate derivative	Silica surface was modified by a sequential reaction of preactivated silica gel with chloropropyl silica, 3-chloropropyltriethoxysilane and ethylenediamine (EDA) or diethylenetriamine (DETA) or triethylenetetramine (TETA) followed by treatment with carbon disulfide for selective solid phase extraction of mercury (II)	(Oksana et al., 2004)
1-Allyl-3-propylthiourea	High adsorption capacity for mercury ions	(Antochshuk et al., 2002)
Amidinothiourea	Cyanoethylaminopropyl silica obtained from reaction of aminopropyl silica gel and acrylonitrile was treated with NH_4SCN to produce amidinothioureido silica gel containing amidine and thiourea functional groups. It is found to extract Ag^+ , Au^{3+} and Pd^{2+} in nano scale	(Zhang et al., 2002)
Thiourea dioxide TUD	Acetalization of aldehydes. NCS with thiourea as highly efficient catalysts for acetalization of aldehyde. 2.0 mmol of aldehyde, 5 mol % NCS 2 mol % Thiourea, MeOH (6 cm^3), 23 °C, tert-butylhydroperoxide TBHP as oxidant for 1 hour	(Mei et al., 2009)
Proline-amino thioureas	Self-assembled proline-amino thioureas as efficient organocatalysts for the asymmetric Michael addition of aldehydes to nitroolefins. Nitrostyrene (0.1 mmol), aldehyde (0.3 mmol), L-proline (10 mol %) and thiourea (10 mol %) in 0.5 mL of toluene at 0 °C	(Wang et al., 2010)

9-thiourea epiquinine heterogeneous Supported by mesoporous SBA-15 and MCM-41 materials	Stepwise fabrication and architecture of heterogeneous 9-thiourea epiquinine catalyst with excellent enantioselectivity in the asymmetric Friedel–Crafts reaction of indoles with imines. Asymmetric Friedel-Crafts reaction of indoles with imines. (93 ee) 77 (99) 78 (96)	(Yu et al., 2008)
Magnetically separable nano CuFe ₂ O ₄	An efficient and reusable heterogeneous catalyst for the green synthesis of thiiranes from epoxides with thiourea. 34–45 min 80-90 % yields. The epoxide was converted to thiirane.	(Eisavi et al., 2016)
6-amino-1,3-dimethyl uracil, aromatic aldehydes, and 1,3-dicarbonyl compound catalyzed by thiourea dioxide in aqueous media.	6-Amino-1,3-dimethyl uracil (3 mmol), aldehyde (3.5 mmol), 1,3-dicarbonyl compound (3.5mmol), TUD (2 mol %) in water (2 ml) at 50 °C under nitrogen Atmosphere for 8 hours reaction. 94 % yield.	(Verma and Jain, 2012)
3-(1-thiouredo)propyl functionalised silica	Online preconcentration and separation of Ag ⁺ , Au ³⁺ and Pd ₂	(Liu and Chen, 2000)
Hybrid inorganic–organic xerogels (XGPtu)	hydrogenation of phenylacetylene (Pd) and hydroformylation of styrene, but metal leaching occurred, even if to a limited extent. Styrene to iso- aldehyde. 92 % yield.	(Cauzzi et al., 2000)
[Rh(cod) ₂] BF ₄ Hydroformylation of styrene by [Rh(cod) ₂] BF ₄ with thiourea:	Conditions: [Rh(cod) ₂] BF ₄ 5.10 ⁻⁵ mol; toluenes:10 ml; styrene :Thiourea: Rh; 350:1:1, CO ₂ + H ₂ (1:1) 40 bar, T:40 °C, time:18 h. Solvent, TH. Styrene to aldehyde (7 % ee) 40 % yield.	(Breuzard et al., 2000)



Cobalt metal complex of
carbonyl thiourea derivatives



Synthesis, crystallography and catalytic activity. Oxidation of alcohols or ketone in presence of TBHP at 80 °C -TBHP was found to be the best as it gave acetophenone. Alcohol to aldehyde. 93 %.

(Gunasekaran et al.,
2012)

1.6 Primary, secondary and tertiary amine in reactions

All organic ligands in this research were identified as secondary amine. However, Wang and Shantz, (2010) and colleagues investigated the effects of organoamine type (primary, secondary, tertiary), amine density, and the presence of silanol groups on the nitroaldol reaction by preparing a series of amine-based MCM-41 materials (Fig. 1.13). The authors also claimed that the best results were obtained when the secondary amines were used. They additionally found that an expansion in the quantity of amine loading has brought a lessening in catalytic activity. One noteworthy point is that the capping of silanols with trimethylsilyl groups reduced the catalytic activity for nearly all samples which indicates that the cooperative effect of surface silanols with amine groups.

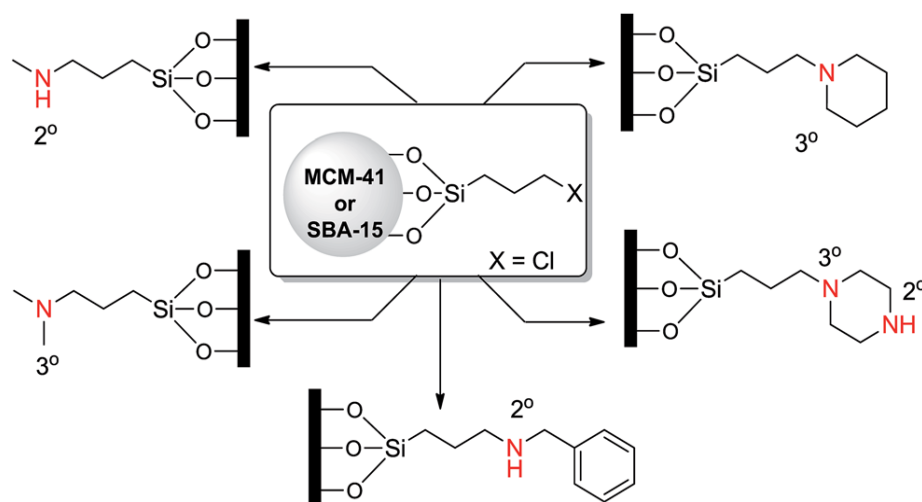


Fig. 1.13: Scheme of secondary and tertiary amine in reactions.

1.7 Limonene

R-Limonene is a colourless oil that is sparingly soluble in water with a sweet orange smell. Commercially, the terpene is mostly obtained from waste orange peel (dry orange peel waste contains 3.8 wt % of R-limonene on a dry weight basis) (Pourbafrani et al., 2010) as shown in Fig. 1.14.



Fig. 1.14: Orange essential oil from orange peel obtained at room temperature after centrifugation of the water oil emulsion. (Image courtesy of (Pourbafrani et al., 2010)).

Today, R-limonene is obtained as a by-product of citric fruit juice processing, mainly by a cold process involving centrifugal separation or by steam distillation. Due to the existence of a chiral center in the chemical structure of limonene (carbon 4. Fig. 1.15), this compound has two enantiomers with optical configurations R and S (Wroblecka et al., 2016). Orange peels are the main source of R-limonene while lime peels mostly contain S-limonene (Wroblecka et al., 2014).

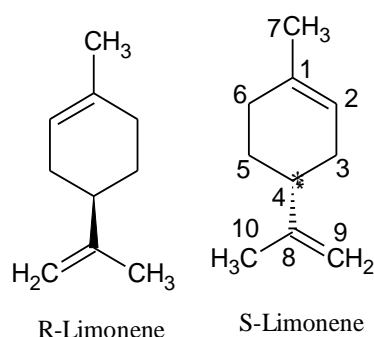


Fig. 1.15: Stereoisomer of limonene with chiral center denoted as (*) at carbon 4.

Limonene can be attained from more than 300 plants. It was one of the regular terpene. It was extricated from citrus oil which is produced 30,000 tones for every year. It was generally utilized as a feedstock. R-limonene has a solid aroma similar to oranges. The production of limonene in Brazil is about 12,500 tonnes per